Title

Stem cell therapy for skin regeneration using mesenchymal stem cells derived from the progeroid Werner syndrome-specific iPS cells

Authors

Shinichiro Funayama[1], Hisaya Kato[1,2*], Hiyori Kaneko[1,2], Kentaro Kosaka[3,4], Daisuke Sawada[1,5], Aki Takada-Watanabe[1], Takuya Minamizuka[1,2], Yusuke Baba[1,6], Masaya Koshizaka[1,2], Akira Shimamoto[7], Yasuo Ouchi[3,8], Atsushi Iwama[9], Yusuke Endo[10], Naoya Takayama[3], Koji Eto[3,11], Yoshiro Maezawa[1,2], Koutaro Yokote[1,2]

Affiliations

[1]Department of Endocrinology, Hematology and Gerontology, Chiba University Graduate School of Medicine, Chiba, Japan

[2]Division of Diabetes, Metabolism and Endocrinology, Chiba University Hospital, Chiba, Japan

[3]Department of Regenerative Medicine, Chiba University Graduate School of Medicine, Chiba, Japan

[4]Department of Plastic, Reconstructive, and Aesthetic Surgery, Chiba University Graduate School of Medicine, Chiba, Japan

[5]Department of Pediatrics, Chiba University Graduate School of Medicine, Chiba, Japan

[6]Department of Medicine, Division of Diabetes, Endocrinology and Metabolism, Kimitsu Chuo Hospital, Kisarazu, Chiba, Japan

[7]Department of Regenerative Medicine Research, Faculty of Pharmaceutical Sciences, Sanyo-Onoda City University, Sanyo-Onoda, Yamaguchi, Japan

[8]Gene Expression Laboratory, Salk Institute for Biological Studies, La Jolla, CA, USA

[9]Division of Stem Cell and Molecular Medicine, Center for Stem Cell Biology and Regenerative Medicine, The Institute of Medical Science, The University of Tokyo, Tokyo, Japan

[10]Laboratory of Medical Omics Research, KAZUSA DNA Research Institute, Kisarazu, Chiba, Japan

[11]Department of Clinical Application, Center for iPS Cell Research and Application (CiRA), Kyoto University, Kyoto, Japan

[*]Corresponding author

Contact Information

Correspondence to: Hisaya Kato

Email: hisayakato@chiba-u.jp

Tel: +81-43-226-2092

Keywords

Werner syndrome, wound healing, mesenchymal stem cell, iPS cell, aging

Abstract

Adult progeria, Werner syndrome (WS), is an autosomal recessive disorder that develops accelerated aging-associated symptoms after puberty. Refractory skin ulcer of limbs, which is one of the symptoms specific to WS, is seriously painful and sometimes results in amputation. In recent years, cell therapy using mesenchymal stem cells (MSCs) has been attracting attention; however, the effect of WS-derived MSCs on skin ulcers is still unclear. In this study, we generated iPS cells from a patient with WS and a normal subject, differentiated them into MSCs (WS- and NM-iMSC, respectively), and performed cell therapy to a refractory skin ulcer mouse model. As a result, WS-iMSC recapitulated premature senescence phenotypes in vitro. Upon subcutaneous injection around the wounds of mice, WS-iMSC was significantly inferior in wound healing effect compared to NM-iMSC. Proteome and transcriptome analysis revealed altered expression of genes related to angiogenesis, inflammation, and proliferation in WS-iMSC with remarkable downregulation of VEGF, a potent angiogenic factor. In addition, simultaneous administration of recombinant human VEGF and WS-iMSC improved the wound healing effect in vivo. These

55 results indicate that the expression of angiogenic factors is reduced in WS-iMSC, and its

56 supplementation restores the wound healing ability. This finding may pave the way to develop the

57 treatment of intractable skin ulcers of WS.

58

Introduction

Werner syndrome (WS), caused by mutation of a RecQ type helicase gene *WRN*, is an autosomal recessive progeroid syndrome that causes various signs of accelerated aging after puberty, including bilateral cataracts, graying and loss of hair, type 2 diabetes, sarcopenia, dyslipidemia, arteriosclerosis, and malignant tumors [1, 2]. In addition to these symptoms, WS patients exhibit disease-specific phenotypes such as calcification of the Achilles tendon, refractory skin ulcers, and high susceptibility to non-epithelial tumors, e.g., sarcomas and hematological malignancies [3, 4]. Among those, refractory painful skin ulcers occur in about 70% of WS patients and often lead to amputation of the lower limbs accompanied by severe pain and osteomyelitis, which result in remarkably reduced patient quality of life [5]. Owing to the lack of a fundamental cure for this condition, the development of a treatment strategy is urgently needed.

Mesenchymal stem cells (MSCs) are somatic stem cells that possess the ability to differentiate into mesenchymal lineages, such as osteocytes, chondrocytes, and adipocytes [6-8]. MSCs have been clinically applied for a wide range of diseases and reported to be effective for graft-versus-host disease, stroke, multiple sclerosis, and diabetic skin ulcers [9-12]. Therefore, the clinical application of MSCs is considered a promising tool for regenerative medicine [13]. On the other

77 hand, MSCs derived from aged mice reportedly had reduced wound healing effects compared to
78 those derived from young mice [14]. Related to this issue, previous reports suggested MSCs
79 derived from human *WRN* knock-out embryonic stem cells exhibited premature senescence
80 phenotypes [15]. Taken together, although treatment with MSCs may have beneficial effects for
81 refractory skin ulcers in WS patients, MSCs derived from WS patients are considered to have
82 decreased wound healing effects than those derived from normal individuals because of
83 accelerated senescence. However, the effect of MSCs from WS on ulcer treatment remains to be
84 elucidated.
85
86 To clarify the skin regenerative effect of MSCs from WS, we generated iPS cells from a normal
87 subject and a patient with WS, differentiated them into MSCs (NM- and WS-iMSC,
88 respectively), and performed cell transplantation using a refractory skin ulcer mouse model.
89

Results

Generation of NM- and WS-iPSC

iPSCs were generated from a normal individual and a patient with WS as previously described [16]. They showed iPSC-like morphologies and the capability of embryoid body formation (Supplementary Figure 1A, B). Gene expression analysis revealed the downregulation of pluripotency genes and upregulation of genes of three germ layers upon differentiation (Supplementary Figure 1C). Sanger-sequencing showed compound heterozygous *WRN* mutation, c.3139-1G>C plus c.3446delA, in WS-iPSC (Supplementary Figure 1D). Thus, we successfully generated NM- and WS-iPSC.

WS-iMSC recapitulated premature senescence phenotypes in vitro

Derivation of iMSCs was conducted according to the previous report with modification [17]. Derived iMSCs exhibited spindle-shaped MSC-like morphologies (Supplementary Figure 2A). They were positive for CD73, CD90, and CD105 and possessed adipogenic, chondrogenic, and osteogenic potentials (Supplementary Figure 2B, C). During the long-term culture, WS-iMSC showed decreased proliferative capacity compared to NM-iMSC (Figure 1A). The analysis of telomere length displayed shortened telomeres in WS-iMSC (Figure 1B). SA-β-gal analysis disclosed a significantly increased number of senescent cells in WS-iMSC (Figure 1C, D). These

results indicate that WS-iMSC recapitulated premature senescence phenotypes in vitro.

WS-iMSC exhibited reduced wound healing effects compared to NM-iMSC

Refractory skin ulcer mouse models were generated by administering streptozotocin (STZ) to severe combined immunodeficient (SCID) mice and creating a wound on their back, as previously reported (Figure 2A) [18]. To determine the wound healing effects of iMSCs, NM- and WS-iMSC suspended in hyaluronic acid were subcutaneously injected into the area around the wound, and wound sizes were tracked for 14 days. As a result, mice administered NM-iMSC showed significantly decreased wound size compared to the groups of vehicle and WS-iMSC on day 14 (Figure 2B, C). Consistent with this finding, attenuated epidermal and dermal thickness was observed in mice administered WS-iMSC (Figure 2D, E, F, G). These results suggest that WS-iMSC possesses insufficient wound healing effects compared to NM-iMSC.

NM-iMSC facilitated angiogenesis

To assess the angiogenic effects of iMSCs, distributions of mouse Pecam-1 and Vegf expression in dermal skin sections on day 14 were evaluated using the in situ hybridization method. The dermis of mice administered NM-iMSC showed increased and decreased expression of Pecam-1 and Vegf, respectively (Figure 3A, B, C). On the other hand, mice administered WS-iMSC and

126 vehicle exhibited opposite outcomes, meaningly expressions of decreased Pecam-1 and
127 increased Vegf in the dermis (Figure 3A, B, C). Conversely, in the analysis of epidermis,
128 expression of Vegf was elevated in mice administered NM-iMSC and reduced in those of WS-
129 iMSC and vehicle (Figure 3D, E). These findings suggest that the angiogenesis was facilitated
130 by NM-iMSC, while the distribution of Vegf expression in the skin after the administration of
131 WS-iMSC is distinct from that of NM-iMSC.
132
133 ***NM-iMSC promoted the migratory effect of WS-fibroblasts compared to WS-iMSC in vitro***
134 Fibroblasts are responsible for producing extracellular matrix to promote angiogenesis [19].
135 Further, fibroblasts have pivotal roles in the wound healing process at the cell proliferation stage
136 [20]. Rapid migration of fibroblasts to the wound site and their proliferation are major
137 components in the acceleration of wound healing [21-23]. Thus, we conducted a co-culture
138 experiment to determine whether co-culturing fibroblasts with NM- or WS-iMSC can promote
139 their migration ability in vitro using Transwell. As a result, there was no difference in the
140 migration ability between dermal fibroblasts from a normal subject (NM-fibroblasts) co-
141 cultured with NM-iMSC and those co-cultured with WS-iMSC (Figure 4A, B). However, the
142 migration ability of fibroblasts from a WS patient (WS-fibroblasts) was significantly reduced
143 when co-cultured with WS-iMSC compared to NM-iMSC (Figure 4A, B). These results suggest

144 that WS-iMSC is inferior to NM-iMSC in its ability to secrete factors that promote the
145 migration of WS-fibroblasts.
146
147 ***NM- and WS-iMSC showed distinct secretome regarding wound healing***
148 MSCs are known to promote angiogenesis and cell proliferation by secreting various cytokines
149 and chemokines [24, 25]. Based on the above results of co-culture experiments, the secreted
150 factors from iMSCs were assumed to be associated with fibroblasts migration and wound
151 healing. Therefore, we carried out a proteome analysis of the culture supernatant of iMSCs to
152 clarify their wound healing-associated secretome. As a result, WS-iMSC had significantly
153 increased secretion of the inflammation-related factors; IL-8, MCP-1, Pentraxin3, and MMP-9
154 compared to NM-iMSC (Figure 5A, B, C). On the other hand, the secretion of proteins related
155 to cell proliferation, such as Activin A, IGFBP-3, and VEGF, were significantly upregulated in
156 NM-iMSC (Figure 5A, B, C). Indeed, enzyme-linked immunosorbent assay confirmed
157 significantly lower VEGF secretion in WS-iMSC than in NM-iMSC (Figure 5D). These
158 findings suggest that NM-iMSC and WS-iMSC have distinct secretomes associated with wound
159 healing.
160
161 ***Gene expression profiles related to angiogenesis and inflammation were altered in WS-iMSC***

Next, we evaluated the transcriptome of NM- and WS-iMSC via RNA-sequence. As a consequence, we extracted 1,114 and 886 genes that were respectively downregulated or upregulated in WS-iMSC compared to NM-iMSC (Figure 6A). Enrichment analysis revealed genes involved in chromosome segregation and cell division were downregulated in WS-iMSC, while those of anatomical structure morphogenesis and regulation of multicellular organismal process were upregulated (Figure 6B). Especially, the expression levels of genes associated with angiogenesis and inflammation, such as VEGFA, CXCL8, etc., were remarkably altered (Supplementary Table). qRT-PCR confirmed significantly different gene expression profiles of the above genes between NM- and WS-iMSC (Figure 6C). These findings might be associated with the attenuated regenerative capacity of the refractory skin ulcer in WS-iMSC.

VEGF supplementation improved the wound healing effect of WS-iMSC

VEGF is a potent angiogenic factor and is also essential in wound healing [26, 27]. Since VEGF expression was reduced in WS-iMSC, we speculated that VEGF supplementation might improve the wound healing effect of WS-iMSC. Therefore, WS-iMSC and recombinant human VEGF were co-injected around the wound of the refractory skin ulcer mouse model. As a result, the wound area on day 10 was significantly reduced in the VEGF injected group (Figure 7A, B)

179 compared to WS-iMSC alone. From these results, the decreased wound healing ability of WS-

180 iMSC might attribute to the deficiency of VEGF secretion.

181

Discussion

In this study, we demonstrated the difference in wound healing efficacy between NM- and WS-iMSC when administered into a refractory skin ulcer mouse model. WS-iMSC manifested premature senescence phenotypes in vitro and weaker wound healing effects compared to NM-iMSC resulting in thinner epidermal and dermal layers in injected mice. Further, mice administered WS-iMSC had decreased and increased expression of mouse Pecam-1 and Vegf in the dermis, respectively, and, in contrast, decreased Vegf expression in the epidermis compared to those administered NM-iMSC. WS-fibroblasts co-cultured with WS-iMSC exhibited reduced migration ability in vitro compared to those co-cultured with NM-iMSC. The proteome analysis revealed significantly reduced VEGF secretion in WS-iMSC. The transcriptome analysis also confirmed significantly lower expression of genes involved in cell proliferation, blood vessels, and inflammation, including VEGFA, in WS-iMSC. Indeed, VEGF supplementation restored the wound healing effect of WS-iMSC.

There are four phases in wound healing: hemostasis, inflammation, proliferation, and remodeling, and various chemokines and cytokines are secreted in each phase [28]. Among those, it is well established that VEGF plays one of the most important roles in angiogenesis [29]. Previous reports suggest that VEGF secreted by myeloid cells and fibroblasts is highly

200 expressed in the dermis in the early stages of wound healing to promote angiogenesis, but its
201 expression shifts to the epidermis in the late stage as keratinocytes migrate onto granulation
202 tissue [28-30]. Therefore, the observed difference in our study in the expression distribution of
203 Vegf in skin sections of mice administered NM- and WS-iMSC might indicate the delayed
204 progression of the wound healing phase in mice administered WS-iMSC.
205
206 The relationship between VEGF and the therapeutic effects of MSCs has been demonstrated in
207 several previous studies. Concomitant injection of MSCs and VEGF reduced the infarct size and
208 preserved ejection fraction in a mouse model of acute myocardial infarction [31]. MSCs
209 overexpressing VEGF demonstrated to promote the migration of vascular endothelial cells and
210 increase vascular density and blood flow in hindlimb ischemic mice [32]. Of note, VEGF
211 proved to be effective in prolonging the MSC survival at the injected site [33]. These findings
212 not only indicate that VEGF secreted by MSCs plays an important role in promoting
213 angiogenesis but also suggest a protective effect of VEGF for MSCs. In the present study, RNA
214 sequencing and proteome analysis revealed significantly lower VEGF expression in WS-iMSC
215 than in NM-iMSC, and simultaneous injection of VEGF and WS-iMSC improved wound
216 healing ability. Therefore, the decreased secretion of VEGF in WS-iMSC might have

217 contributed to the delay in wound healing, and its restoration might ameliorate the regenerative
218 ability of WS-iMSC.
219
220 Few reports have described the relationship between VEGF and WS so far. Goto M, et al.
221 reported an increased serum VEGF level in WS patients [34]. Another study indicated that
222 knockdown of the WRN gene under a hypoxic condition led to an increased VEGF expression
223 due to HIF1α augmentation in HeLa cells [35]. On the other hand, MSCs collected from older
224 people have reportedly decreased VEGF secretion [36]. WS-iMSC showed reduced VEGF
225 secretion in our study, but further studies are needed to elucidate the underlying mechanism.
226
227 In this study, WS-iMSC exhibited reduced treatment capacity to refractory skin ulcers, probably
228 due to the decreased secretion of VEGF. These findings might contribute to the elucidation of
229 disease pathogenesis and the development of novel therapeutic approaches in the near future.

Materials and Methods

iPSC and iMSC induction and cell culture

Cell culture was performed at 37 °C with 5% CO_2 under humidified air. iPSCs were generated from a male normal individual and a male patient with WS in their 50s as previously described [16]. Derivation of iMSCs was conducted according to the previous report with modification [17]. Briefly, embryoid bodies were cultured in collagen type IV-coated plates (Corning, 354416) with MSC derivation medium (alpha-MEM (Invitrogen), 10% FBS (Hyclone), Antibiotic-Antimycotic (Gibco, 15240062), 100 nM dexamethasone (Sigma-Aldrich), 50 uM L-ascorbic acid 2-phosphate sesquimagnesium salt hydrate (Sigma-Aldrich, A8960-5G)). After five days, cells were passaged on collagen type I (Nitta Gelatin, Cellmatrix Type I-C) fibril-coated plate (defined as passage 0, population doubling level 0) and cultured in expansion medium (alpha-MEM (Invitrogen), 10% FBS (Hyclone), Antibiotic-Antimycotic (Gibco, 15240062), non-essential amino acids (Invitrogen, 11140-050)). The medium change was performed every 3 days. When reaching subconfluent, cells were passaged at a 1:4 split ratio. To draw the growth curve, 5×10^4 of NM- and WS-iMSC at PDL5 (P3) were seeded on collagen I coated 6 well plates (Iwaki, 4810-010). 5×10^4 cells were counted and passaged every 4 to 5 days until P12. Dermal fibroblasts, established from a male normal individual or a male WS patient in their 40s, were cultured in DMEM (043-30085, Wako) supplemented with 10% FBS (10270106, Gibco) and antibiotic (15240062, Gibco)

248 in normal culture dishes (TR4002, TrueLine) at 37 °C with 5% CO_2. The cells at subconfluency
249 were passaged at a ratio of 1:4, and those with population doublings (PD) of 8 to 18 were used in
250 the experiment.
251
252 ***Fluorescence-activated cell sorting (FACS)***
253 Surface markers of MSCs were analyzed by flow cytometer (BD FACSCanto II). In detail, MSCs
254 were dispersed using Trypsin-EDTA (Gibco, 25200072) and suspended in PBS with 2mM EDTA
255 and 0.5% BSA (Sigma, A3294-50G). Cells were incubated with primary antibodies (anti-CD73
256 (BD Biosciences, 550257), anti-CD90 (BD Biosciences, 555595), and anti-CD105 (eBioscience,
257 17-1057-42)) for 30 min at room temperature and analyzed.
258
259 ***Tri-lineage differentiation***
260 In vitro differentiation potentials of MSCs into three lineages were evaluated by using
261 adipogenesis, chondrogenesis, and osteogenesis differentiation kit (A1007001, A1007101, and
262 A1007201, respectively. All from Gibco) according to the manufacturer's protocols. For each
263 assay, oil red o, alcian blue, and alizarin red stainings (All Sigma) were used, respectively.
264
265 ***Relative telomere length measurement***

For the analysis of the relative telomere length, genomic qPCR was conducted using the SYBR Green PCR master mix (Applied Biosystems), as previously described [37].

Senescence-associated β-galactosidase staining

Senescence-associated β-galactosidase (SA-β-Gal) staining was performed following the manufacturer's instruction (Cell Signaling, 9860S). After staining the nuclear DNA using Hoechst 33,342 (DOJINDO, 346–07951), the positive rate was calculated.

Breeding environment

Mice were housed under a temperature of 24 ± 2°C and humidity of 55 ± 5%, with light exposure from 6:00-18:00 (12-hour automatic lighting). Aspen chips were placed in the plastic cage as bedding, and mice were fed CE-2 (Oriental Yeast Co. Ltd.), a solid feed for mice.

Preparation of refractory skin ulcer model mice and administration of iMSC

Diabetes mellitus was induced in six-week-old severe combined immunodeficient (SCID) mice (C.B17/Icr-scidJcl scid/scid, CLEA Japan, Inc.), as previously described [18]. Briefly, mice were administered 150 mg/kg of streptozotocin (STZ; S0130-1G, Sigma-Aldrich). At three days after STZ administration, the blood glucose (BG) was measured, and mice with BG ≧ 300 mg/dl were

284 considered diabetic immunodeficient mice (DM-SCID). Mice that did not reach the BG of 300
285 mg/dl received a second administration of STZ (150 mg/kg), and their BG was measured three
286 days later.
287
288 Ten-week-old DM-SCID mice were anesthetized, and a 6-mm wound was created on the skin
289 using the Disposable Biopsy Punch (BP-60F, Kai Medical). A donut-shaped rubber sheet with
290 internal and external diameters of 10 mm and 16 mm, respectively, created by cutting out a 1-mm
291 thick silicone rubber sheet (Kyowa Industries), was sewn around the wound of mice. Perme-roll
292 (H24R05, Nitto Medical) was applied for wound dressing.
293
294 Three experimental groups of mice were established: vehicle group, normal group, and WS group.
295 For the vehicle group, 600 μl of sodium hyaluronate (6.66 mg/ml, H0603, Tokyo Chemical
296 Industry) was mixed with 100 μl of DMEM (043-30085, Wako Pure Chemical Industries).
297 Thereafter, a total of 100 μl of the mixture was subcutaneously injected around the wound divided
298 into four points. For the NM and WS groups, 7.0×10^6 NM- or WS-iMSC suspended in 100 μl of
299 DMEM was further suspended in 600 μl of hyaluronic acid. Thereafter, a total of 100 μl of cell
300 suspension (including 1.0×10^6 cells) was injected around the wound divided into four points. The
301 wound was photographed on days 0, 3, 7, 10, and 14 after the injection, and mice were dissected

302 on day 14. The wound areas were analyzed using the image analysis software, AreaQ. In the
303 VEGF co-administration experiment, 0.15 ng of human recombinant VEGF (Gibco) were co-
304 injected with 1.0×10^6 cells of WS-iMSC.
305
306 ***Immunohistochemical staining***
307 The skin around the wound was isolated with a disposable biopsy punch (6 mm) at the time of
308 dissection. The isolated skin was then cut into two pieces, one of which was fixed with 4%
309 paraformaldehyde to prepare a paraffin-embedded section (GenoStaff). After deparaffinization
310 and rehydration, the prepared slides were immersed in 10 mM citric acid buffer, autoclaved for
311 antigen activation, and immersed in 3% H2O2/PBS to inhibit the endogenous peroxidase activity.
312 After blocking, anti-Cytokeratin 10 antibodies (ab76318, Abcam) and Alexa Flour 594 (1:1000,
313 A11037, Thermo Fisher) were added to the sections. The sections were sealed with DAPI-
314 containing Fluoro-KEEPER (12745-74, Nacalai Tesque) and analyzed using the image analysis
315 software ImageJ.
316
317 ***HE staining and Masson's trichrome staining***
318 Paraffin-embedded sections were deparaffinized and rehydrated. Thereafter, the sections were
319 stained with Mayer's hematoxylin solution (032-14635, Wako). After staining with eosin solution,

320 the sections were lyophilized and sealed. Masson's trichrome staining was performed by
321 GenoStaff. The sections were analyzed using the image analysis software ImageJ.
322
323 ***In situ hybridization***
324 In situ hybridization was performed using the RNAscope Duplex Color Assay Kit
325 (RNAscope(R)2.5 HD Duplex Reagent Kit, 322430, ACD), according to the product protocol.
326 After baking at 60 °C in a HybEZ oven (HybEZ™ Hybridization System With EZ-Batch Slide
327 System, 321461, ACD), the slides were deparaffinized and rehydrated. After treated with H2O2,
328 the slides were immersed in RNAscope(R) Target Retrieval Reagent (322000, ACD) heated to 100-
329 104 °C for 15 min for antigen activation. Protease treatment of the sections by using Protease Plus
330 was performed at 40 °C for 30 min. The mixture probe, prepared by mixing RNAscope® Probe-
331 Mm-Vegfa-ver2 (412261, ACD) and RNAscope® Probe-Mm-Pecam1-C2 (316721-C2, ACD) at
332 a ratio of 50:1, was added to the sections for hybridization at 40 °C for 2 h. The signal was further
333 amplified by incubation. The Pecam-1 and VEGF signals were stained with red and blue,
334 respectively. The sections were analyzed using the image analysis software ImageJ.
335

336 ***Transwell migration assay***

337 NM- and WS-iMSC were seeded at a density of 6.0×10^4 cells/well in 24-well plates. After

338 culturing for 24 h, a culture insert (for 24-well plates, 8.0 μm, 353097, Corning) was attached to

339 each well, and 2.0×10^4 NM- or WS-fibroblasts were seeded on the insert. After 24 h, cells on

340 top of the insert were removed with a cotton swab, and cells migrated into the bottom of the

341 insert were fixed with 4% paraformaldehyde. The membrane of the insert was removed and

342 attached to a slide, and finally sealed with a DAPI-containing Fluoro-KEEPER. The analysis

343 was performed using the image analysis software ImageJ.

344

345 ***Proteome analysis and Enzyme-linked immunosorbent assay (ELISA)***

346 NM- and WS-iMSC were trypsinized and seeded at a density of 1.5×10^5 cells/well in 12-well

347 plates. After culturing for 24 h, the medium was replaced with 1 ml of MEMα, and cells were

348 cultured for another 24 h. Thereafter, the culture supernatant was collected and stored at -80 °C.

349 For analysis, the Proteome Profiler Human Angiogenesis Array Kit (511-61901, Wako) was used

350 according to the protocol. Blotted membrane was analyzed using ChemiDoc™MP (BIO-RAD)

351 and Image Lab. By using the same samples, we carried out an ELISA, according to the protocol

352 of the VEGF Human ELISA Kit (ab100662, Abcam).

353

354 ***Gene expression analysis***

355 A total of 100,000 NM- and WS-iMSC collected in 1.5-ml tubes were pelleted for storage at -
356 80 °C. RNA was extracted from the cells by using TRIzol(R)Reagent (15596026, ambion),
357 according to the protocol of the PureLink™ RNA Micro Scale Kit (12183016, Thermo Fisher).
358 RNA sequencing was performed by the Kazusa DNA Research Institute. The obtained FASTQ
359 file was mapped to the human genome, GRCh38.99, using STAR (ver.2.7.6a) and RSEM
360 (ver.1.3.3) to obtain the BAM file. The obtained gene count data were analyzed using iDEP [38].
361 Gene clustering was performed by analyzing the top 2,000 genes with variable expression by
362 using k-Means. For qRT-PCR, cDNA was synthesized as previously described [39]. Following
363 probes were used (all from TaqMan); VEGFA, Hs00900055_m1; PDGFB, Hs00966522_m1;
364 FGFR2, Hs01552926_m1; KDR, Hs00911700_m1; IGF2, Hs01005963_m1; CXCL8,
365 Hs00174103_m1; FGF1, Hs01092738_m1; FLT1, Hs01052961_m1; MMP1, Hs00899658_m1;
366 CCL2, Hs00234140_m1; GAPDH, Hs02786624_g1 (internal control).

367

368 ***Study approval***

369 All experiments were approved by the institutional review boards at the Chiba University
370 Graduate School of Medicine (Chiba, Japan). Written informed consent was obtained from
371 study participants before the commencement of this research.

372

373 **Author Contributions**

374 S.F. and H.Kato designed the study, carried out the experiments, analyzed the data, wrote the

375 manuscript, and composed the figures; H.Kaneko, K.K., D.S., A.T.W., T.M., and Y.B., carried

376 out the experiments; M.K., A.S., Y.O., A.I., N.T., and K.E. discussed the data; Y.E. conducted

377 transcriptome analysis; Y.M. and K.Y. designed the study, discussed the data, and managed

378 funding; all authors approved the final version of the manuscript.

379

380 **Acknowledgments**

381 This work was supported by Japan Society for the Promotion of Science (JSPS) KAKENHI

382 under Grant Numbers JP19K23939 (H.Kato), JP20H00524 (K.Y.), JP20K16542 (H.Kato);

383 Japan Agency for Medical Research and Development (AMED) under Grant Numbers

384 JP20bm0804016 (K.Y.), JP20ek0109353 (K.Y.), JP20gm5010002 (K.Y.); Ministry of Health,

385 Labour and Welfare (MHLW) of Japan under Grant Number H30-nanchi-ippan-009 (K.Y.).

386

387 **Conflicts of Interest**

388 All authors declare no potential conflicts of interest in association with this work.

389

References

1. Takemoto, M., et al., *Diagnostic criteria for Werner syndrome based on Japanese nationwide epidemiological survey*. Geriatr Gerontol Int, 2013. **13**(2): p. 475-81.

2. Yokote, K., et al., *WRN Mutation Update: Mutation Spectrum, Patient Registries, and Translational Prospects*. Hum Mutat, 2017. **38**(1): p. 7-15.

3. Oshima, J., J.M. Sidorova, and R.J. Monnat, Jr., *Werner syndrome: Clinical features, pathogenesis and potential therapeutic interventions*. Ageing Res Rev, 2017. **33**: p. 105-114.

4. Onishi, S., et al., *Japanese diabetic patients with Werner syndrome exhibit high incidence of cancer*. Acta Diabetol, 2012. **49 Suppl 1**(Suppl 1): p. S259-60.

5. Koshizaka, M., et al., *Time gap between the onset and diagnosis in Werner syndrome: a nationwide survey and the 2020 registry in Japan*. Aging-Us, 2020. **12**(24): p. 24940-24956.

6. Harris, R.G., et al., *Lack of a fusion requirement for development of bone marrow-derived epithelia*. Science, 2004. **305**(5680): p. 90-3.

7. Volarevic, V., et al., *Concise review: Mesenchymal stem cell treatment of the complications of diabetes mellitus*. Stem Cells, 2011. **29**(1): p. 5-10.

8. Petersen, B.E., et al., *Bone marrow as a potential source of hepatic oval cells*. Science,

1999. **284**(5417): p. 1168-70.

9. Wang, L., et al., *Efficacy and safety of mesenchymal stromal cells for the prophylaxis of chronic graft-versus-host disease after allogeneic hematopoietic stem cell transplantation: a meta-analysis of randomized controlled trials*. Ann Hematol, 2018. **97**(10): p. 1941-1950.

10. Petrou, P., et al., *Beneficial effects of autologous mesenchymal stem cell transplantation in active progressive multiple sclerosis*. Brain, 2020.

11. Chen, L., et al., *Multiple cell transplantation based on an intraparenchymal approach for patients with chronic phase stroke*. Cell Transplant, 2013. **22 Suppl 1**: p. S83-91.

12. Lu, D., et al., *Long-Term Outcomes of BMMSC Compared with BMMNC for Treatment of Critical Limb Ischemia and Foot Ulcer in Patients with Diabetes*. Cell Transplant, 2019. **28**(5): p. 645-652.

13. Han, Y., et al., *Mesenchymal Stem Cells for Regenerative Medicine*. Cells, 2019. **8**(8): p. 886.

14. Bruna, F., et al., *Regenerative Potential of Mesenchymal Stromal Cells: Age-Related Changes*. Stem Cells Int, 2016. **2016**: p. 1461648.

15. Zhang, W., et al., *Aging stem cells. A Werner syndrome stem cell model unveils heterochromatin alterations as a driver of human aging*. Science, 2015. **348**(6239): p.

1160-3.

16. Kato, H., et al., *Generation of disease-specific and CRISPR/Cas9-mediated gene-corrected iPS cells from a patient with adult progeria Werner syndrome*. Stem Cell Research, 2021. **53**: p. 102360.

17. Liu, Y., et al., *One-step derivation of mesenchymal stem cell (MSC)-like cells from human pluripotent stem cells on a fibrillar collagen coating*. PLoS One, 2012. **7**(3): p. e33225.

18. Kinoshita, K., et al., *Therapeutic Potential of Adipose-Derived SSEA-3-Positive Muse Cells for Treating Diabetic Skin Ulcers*. Stem Cells Transl Med, 2015. **4**(2): p. 146-55.

19. Newman, A.C., et al., *The requirement for fibroblasts in angiogenesis: fibroblast-derived matrix proteins are essential for endothelial cell lumen formation*. Mol Biol Cell, 2011. **22**(20): p. 3791-800.

20. Desmouliere, A., et al., *Fibroblasts and myofibroblasts in wound healing*. Clinical, Cosmetic and Investigational Dermatology, 2014. **Volume 7**: p. 301-311.

21. Dunnill, C., et al., *Reactive oxygen species (ROS) and wound healing: the functional role of ROS and emerging ROS-modulating technologies for augmentation of the healing process*. Int Wound J, 2017. **14**(1): p. 89-96.

22. Broughton, G., J.E. Janis, and C.E. Attinger, *The basic science of wound healing*. Plast

Reconstr Surg, 2006. **117**(7 Suppl): p. 12S-34S.

23. DeLisser, H.M., *Modulators of endothelial cell filopodia: PECAM-1 joins the club*. Cell Adh Migr, 2011. **5**(1): p. 37-41.

24. Madrigal, M., K.S. Rao, and N.H. Riordan, *A review of therapeutic effects of mesenchymal stem cell secretions and induction of secretory modification by different culture methods*. J Transl Med, 2014. **12**: p. 260.

25. Ren, G., et al., *Concise review: mesenchymal stem cells and translational medicine: emerging issues*. Stem Cells Transl Med, 2012. **1**(1): p. 51-8.

26. Ferrara, N., H.P. Gerber, and J. LeCouter, *The biology of VEGF and its receptors*. Nat Med, 2003. **9**(6): p. 669-76.

27. Bao, P., et al., *The role of vascular endothelial growth factor in wound healing*. J Surg Res, 2009. **153**(2): p. 347-58.

28. Sun, B.K., Z. Siprashvili, and P.A. Khavari, *Advances in skin grafting and treatment of cutaneous wounds*. Science, 2014. **346**(6212): p. 941-5.

29. Johnson, K.E. and T.A. Wilgus, *Vascular Endothelial Growth Factor and Angiogenesis in the Regulation of Cutaneous Wound Repair*. Adv Wound Care (New Rochelle), 2014. **3**(10): p. 647-661.

30. Brown, L.F., et al., *Expression of vascular permeability factor (vascular endothelial*

growth factor) by epidermal keratinocytes during wound healing. J Exp Med, 1992. **176**(5): p. 1375-9.

31. Deuse, T., et al., *Hepatocyte growth factor or vascular endothelial growth factor gene transfer maximizes mesenchymal stem cell-based myocardial salvage after acute myocardial infarction*. Circulation, 2009. **120**(11 Suppl): p. S247-54.

32. Beegle, J.R., et al., *Preclinical evaluation of mesenchymal stem cells overexpressing VEGF to treat critical limb ischemia*. Mol Ther Methods Clin Dev, 2016. **3**: p. 16053.

33. Pons, J., et al., *VEGF improves survival of mesenchymal stem cells in infarcted hearts*. Biochem Biophys Res Commun, 2008. **376**(2): p. 419-22.

34. Goto, M., et al., *Multiplex cytokine analysis of Werner syndrome*. Intractable Rare Dis Res, 2015. **4**(4): p. 190-7.

35. Labbe, A., et al., *The Werner syndrome gene product (WRN): a repressor of hypoxia-inducible factor-1 activity*. Exp Cell Res, 2012. **318**(14): p. 1620-32.

36. Zhang, Y., et al., *Macrophage migration inhibitory factor rejuvenates aged human mesenchymal stem cells and improves myocardial repair*. Aging (Albany NY), 2019. **11**(24): p. 12641-12660.

37. O'Callaghan, N.J. and M. Fenech, *A quantitative PCR method for measuring absolute telomere length*. Biol Proced Online, 2011. **13**(1): p. 3.

38. Ge, S.X., E.W. Son, and R. Yao, *iDEP: an integrated web application for differential expression and pathway analysis of RNA-Seq data*. BMC Bioinformatics, 2018. **19**(1): p. 534.

39. Kato, H., et al., *Fibroblasts from different body parts exhibit distinct phenotypes in adult progeria Werner syndrome*. Aging (Albany NY), 2021. **13**(4): p. 4946-4961.

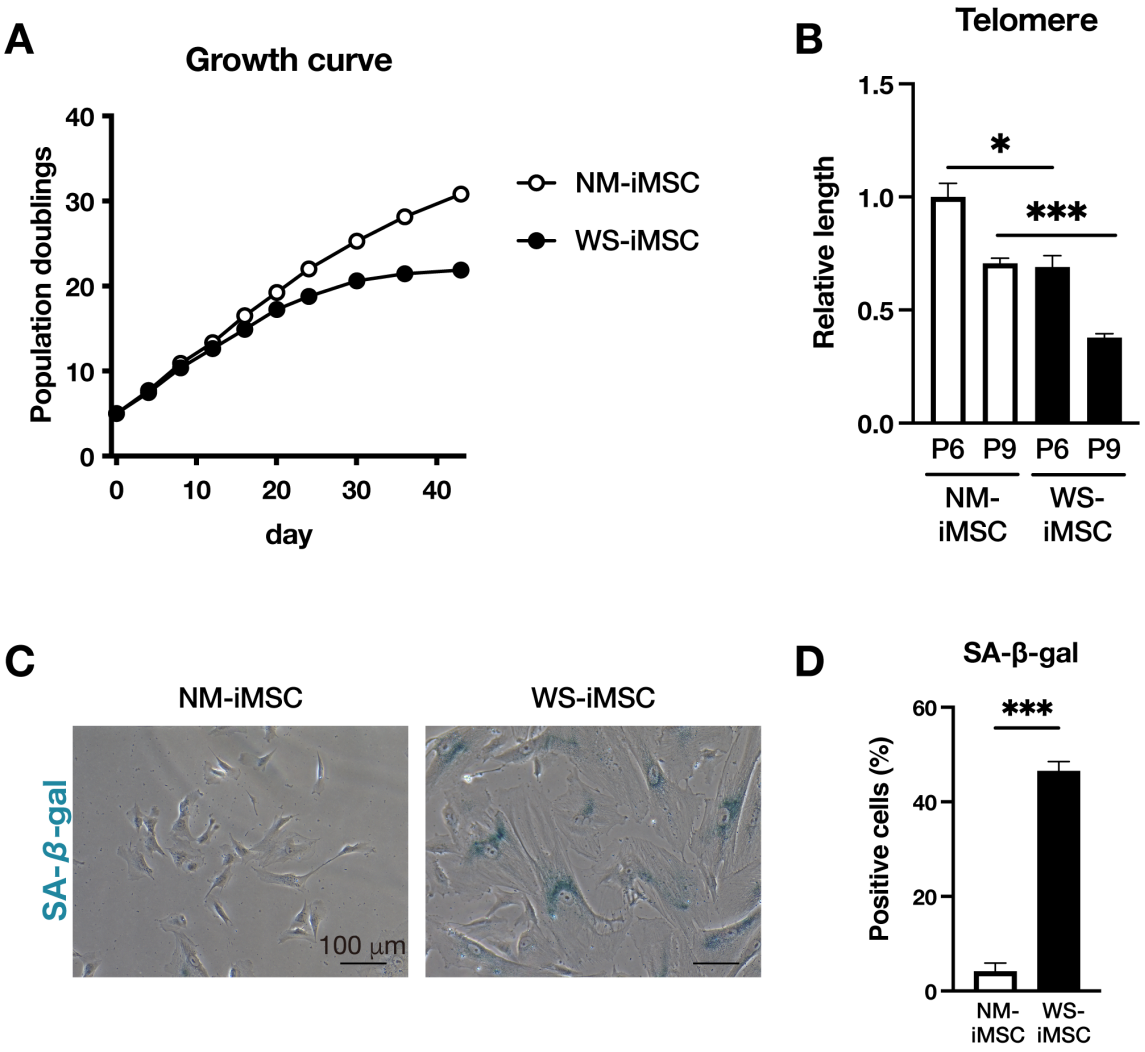

Figure 1. Premature senescence phenotypes of WS-iMSC.

(A) Growth curves of NM- and WS-iMSC. (B) Relative telomere length quantified by qPCR at passages 6 and 9. Data are mean ± SEM of three technical replicates. A student t-test was performed (*p<0.05, ***p<0.001). (C) Representative images of SA-β-gal staining at passage 12. Scale bar = 100 μm. (D) The rate of positive cells related to Figure 1C. More than 200 cells in each group were counted. Data are mean ± SEM of five microscopic views. A student t-test was performed (***p<0.001).

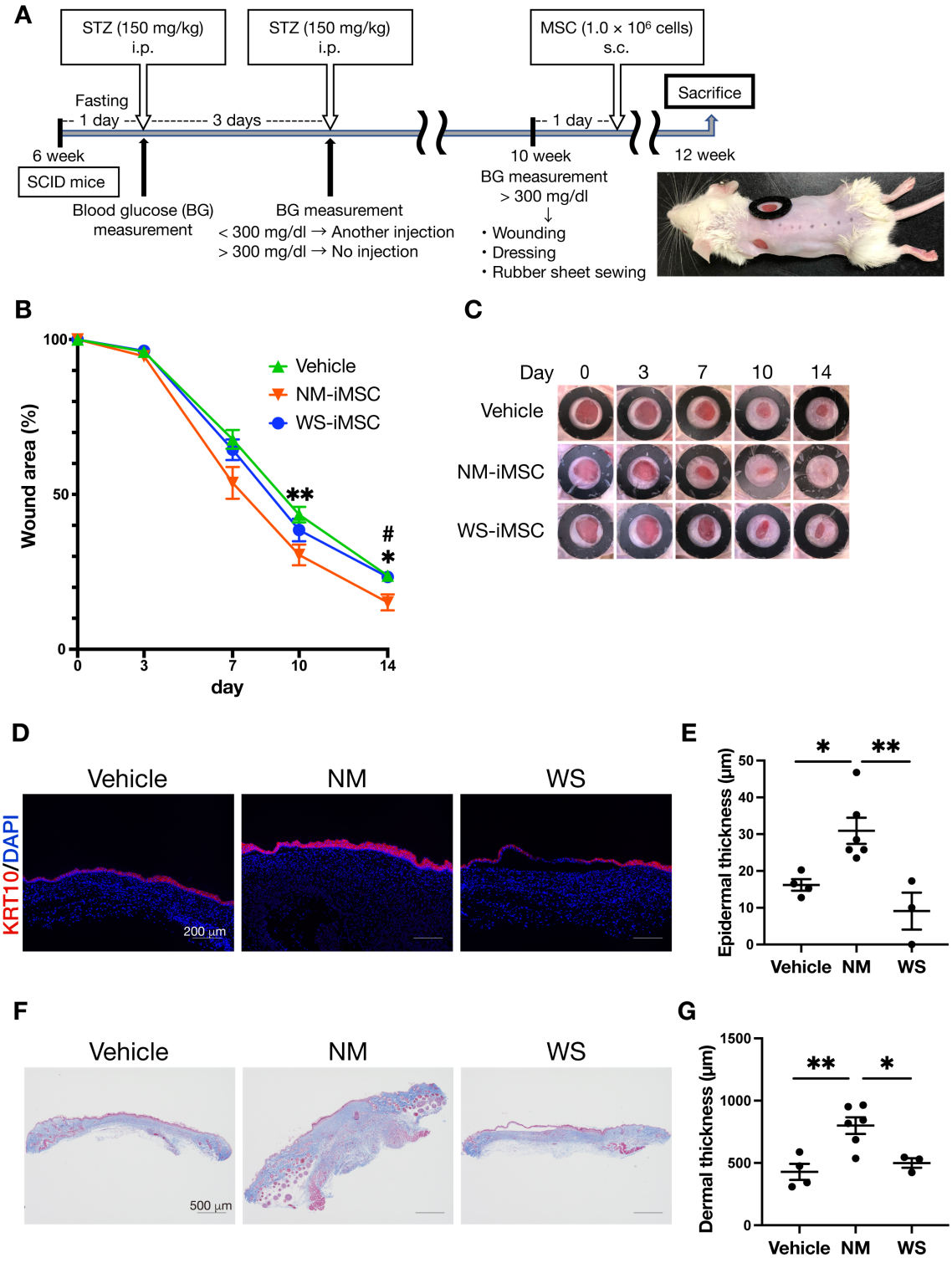

Figure 2. Wound healing effects of refractory skin ulcer mouse model by administering NM- and WS-iMSC.

(A) Scheme representing the production of refractory skin ulcer mouse model and subsequent experiments. (B) Graph showing the rate of wound area from day 0 to 14. Data are mean ± SEM (Veh, n = 8; NM, n = 10; WS, n = 6). A student t-test was performed (*p<0.05, **p<0.01, Veh vs NM-iMSC; #p<0.05, WS-iMSC vs NM-iMSC). (C) Representative pictures of wounds on mice in each group. (D) Representative images of immunohistochemical staining with KRT10 and DAPI of mouse skin sections on day 14. (E) Quantification of epidermal thickness related to Figure 2D. Data are mean ± SEM. A student t-test was performed (*p<0.05, **p<0.01). (F) Representative images of mouse skin sections stained by Masson's trichrome staining method. (G) Quantification of dermal thickness related to Figure 2F. Data are mean ± SEM. A student t-test was performed (*p<0.05, **p<0.01).

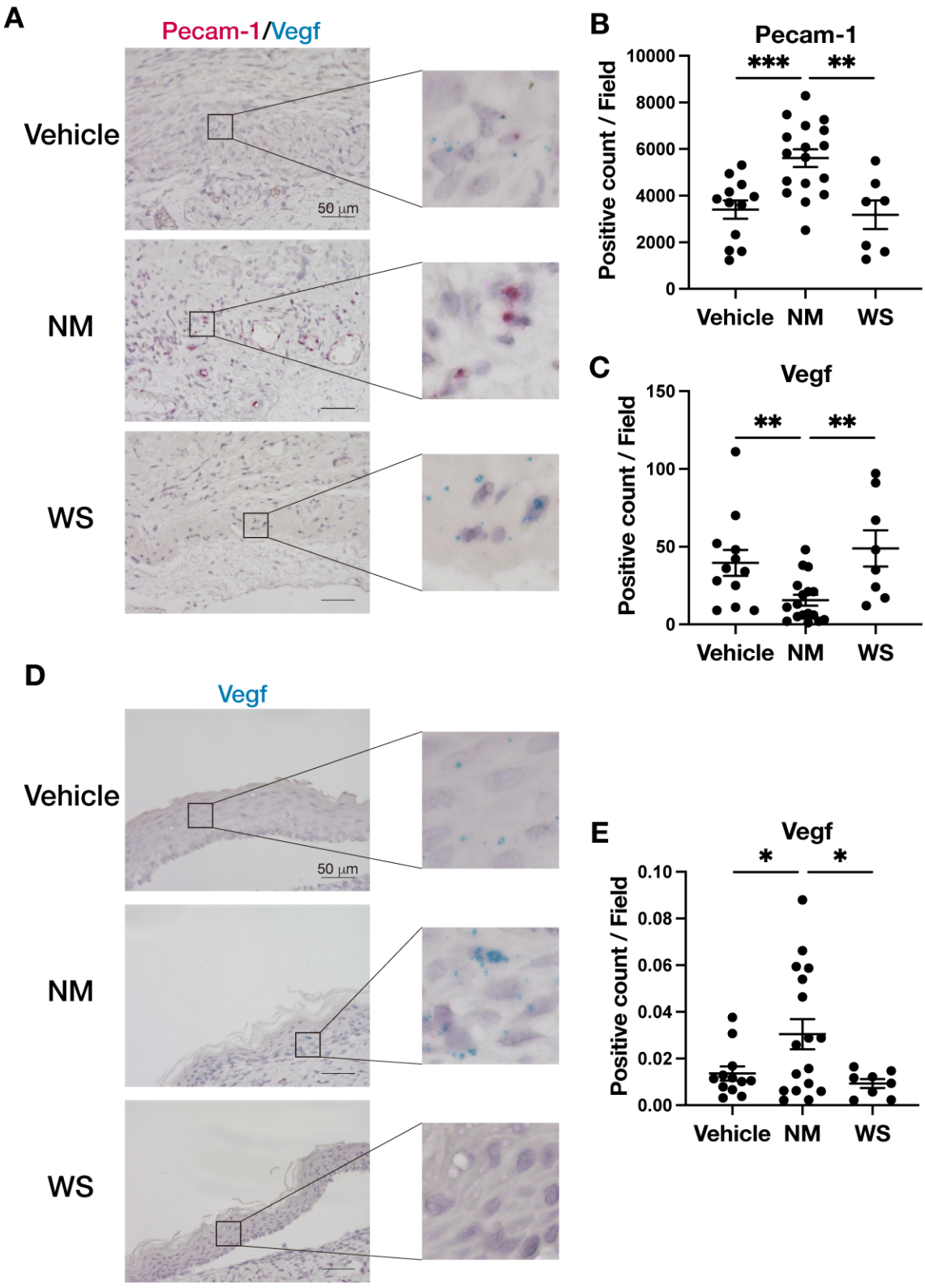

Figure 3. Analysis of Pecam-1 and Vegf expression in dermis and epidermis by in situ hybridization.

511 (A) Representative images of Pecam-1 (red dots) and Vegf (blue dots) in dermal sections of mice
512 on day 14. (B), (C) Quantification of dots positive for Pecam-1 (B) and Vegf (C) related to Figure
513 3A. Data are mean ± SEM. A student t-test was performed (**p<0.01, ***p<0.001). (D)
514 Representative images Vegf (blue dots) in epidermal sections of mice on day 14. (E)
515 Quantification of dots positive for Vegf related to Figure 3D. Data are mean ± SEM. A student t-
516 test was performed (*p<0.05).

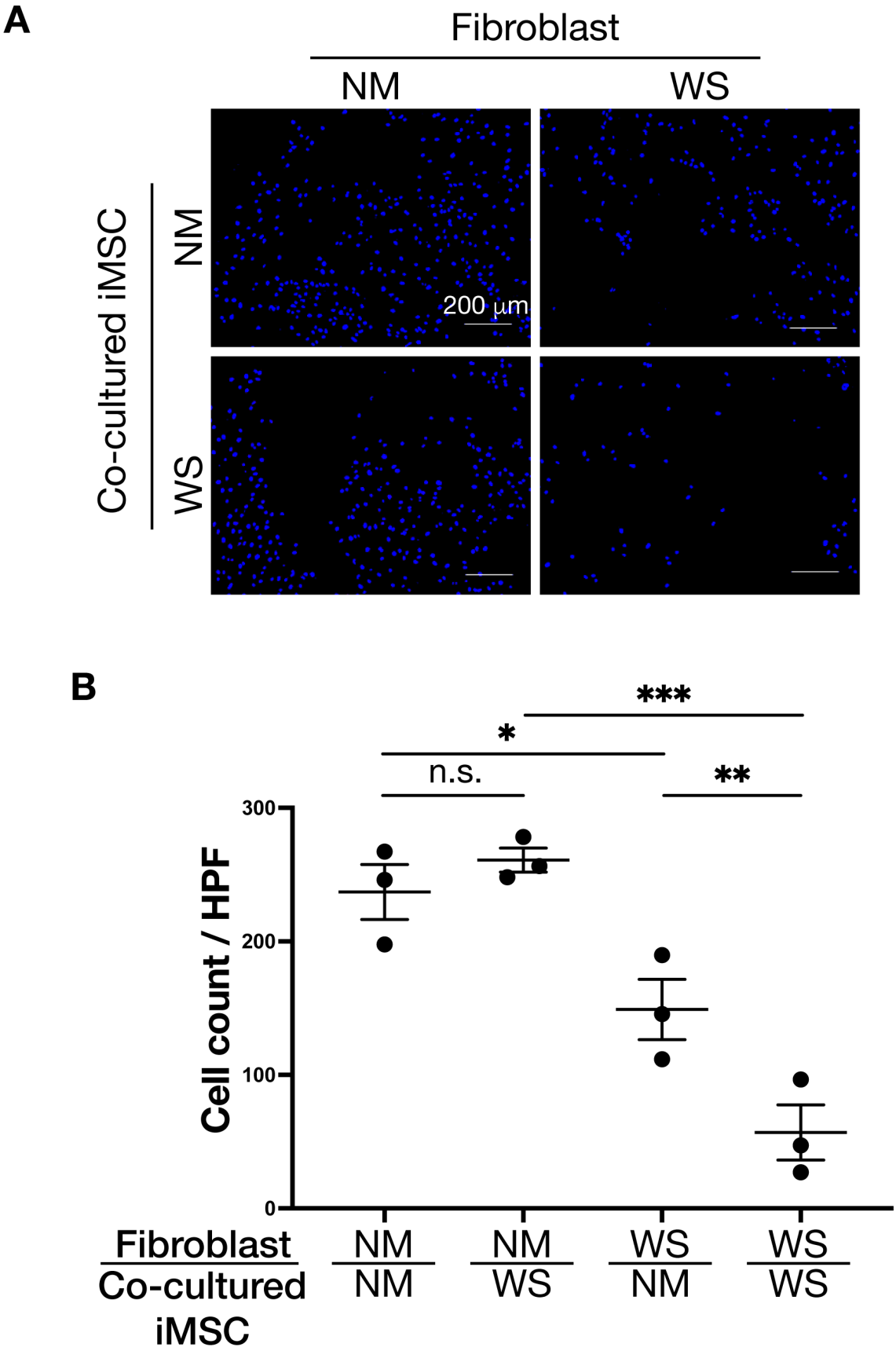

517

Figure 4. Analysis of the migratory ability of fibroblasts co-cultured with NM- and WS-iMSC. (A) Representative images of fibroblasts that migrated beneath the Transwell chamber stained with DAPI after 24-hour co-culturing with NM- and WS-iMSC. (B) Quantification of migrated fibroblasts related to Figure 4A. Data are mean ± SEM (n = 3). A student t-test was performed (n.s., not significant; *p<0.05; **p<0.01; ***p<0.001).

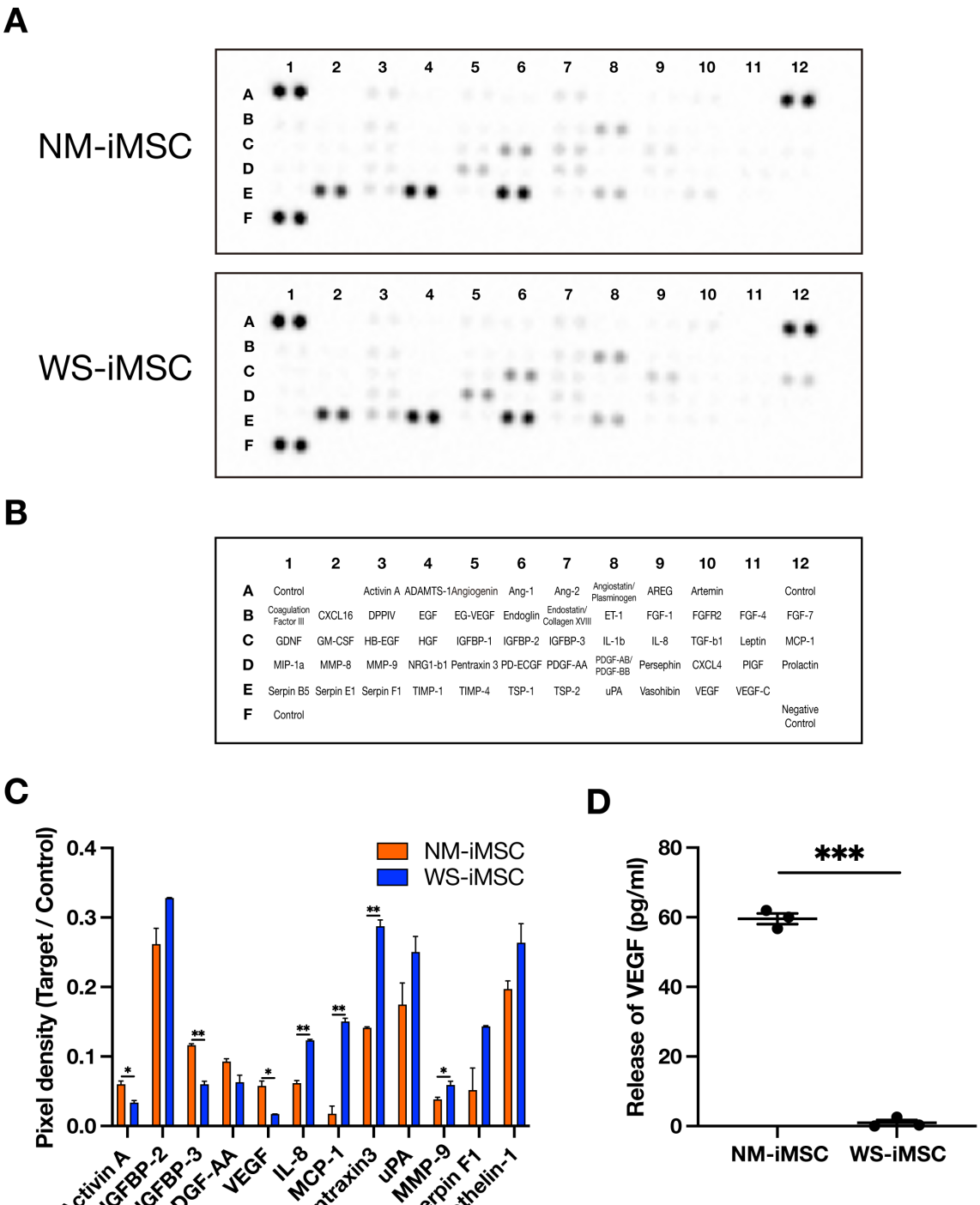

Figure 5. Analysis of secreted factors in NM- and WS-iMSC conditioned medium.

(A) Images of the blotted membrane in proteome analysis of angiogenic factors secreted by NM- and WS-iMSC. (B) Plot table of the membrane in Figure 5A. (C) Quantification of proteome

527 analysis shown in Figure 5A. Data are mean ± SEM. A student t-test was performed (*p<0.05;

528 **p<0.01). (D) The concentration of VEGF in conditioned medium measured by ELISA. Data

529 are mean ± SEM. A student t-test was performed (***p<0.001).

530

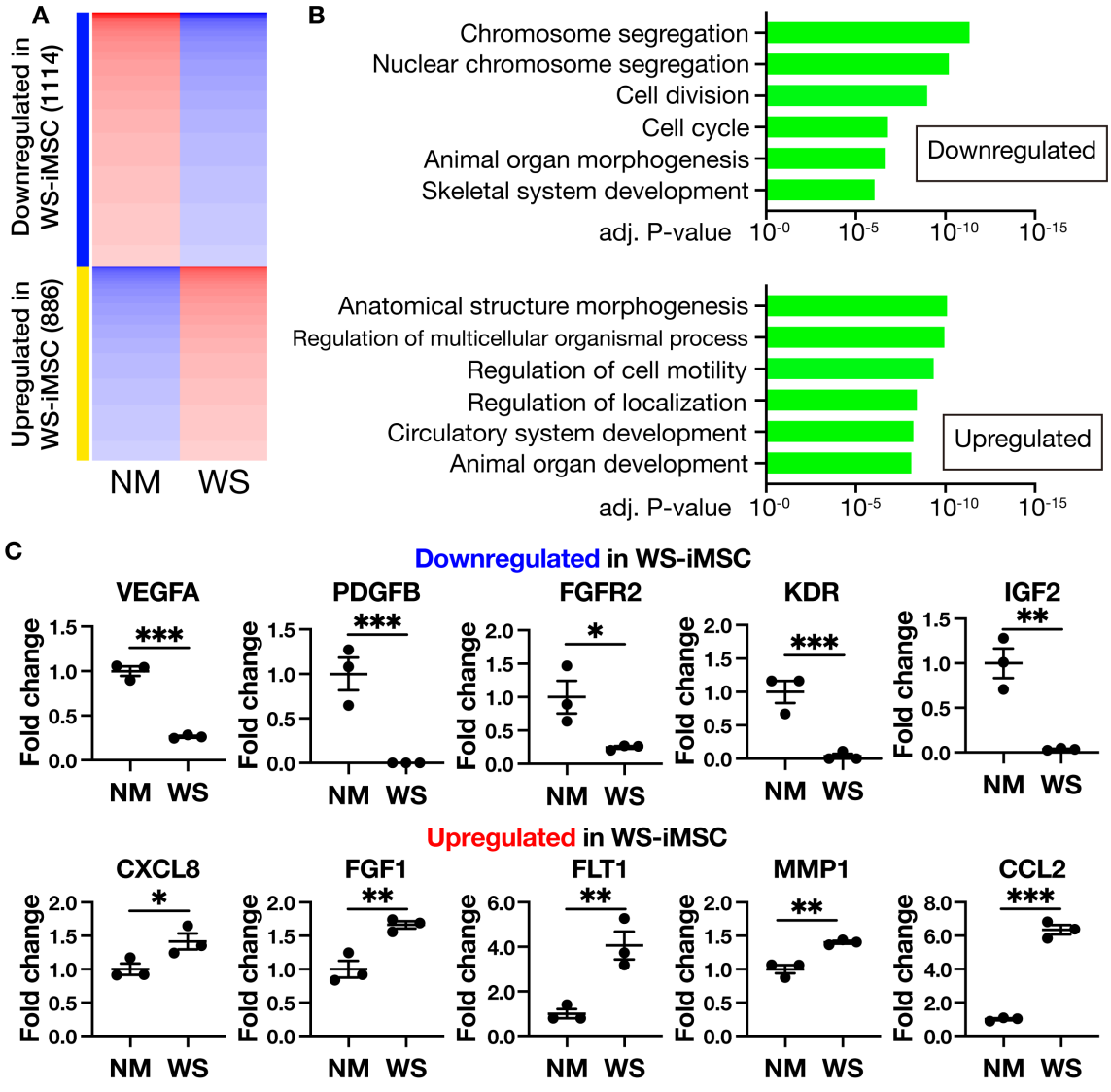

531

532 Figure 6. Gene expression analysis of NM- and WS-iMSC.

533 (A) Heatmap of differentially expressed genes between NM- and WS-iMSC in transcriptome

534 analysis. (B) List of gene ontology (GO: biological process) analysis and corresponding p-values
535 related to Figure 6A. (C) qRT-PCR results of genes related to cell proliferation, angiogenesis, and
536 inflammation. Data are means ± SEM of three technical replicates. A student t-test was performed
537 (*p<0.05; **p<0.01; ***p<0.001).
538

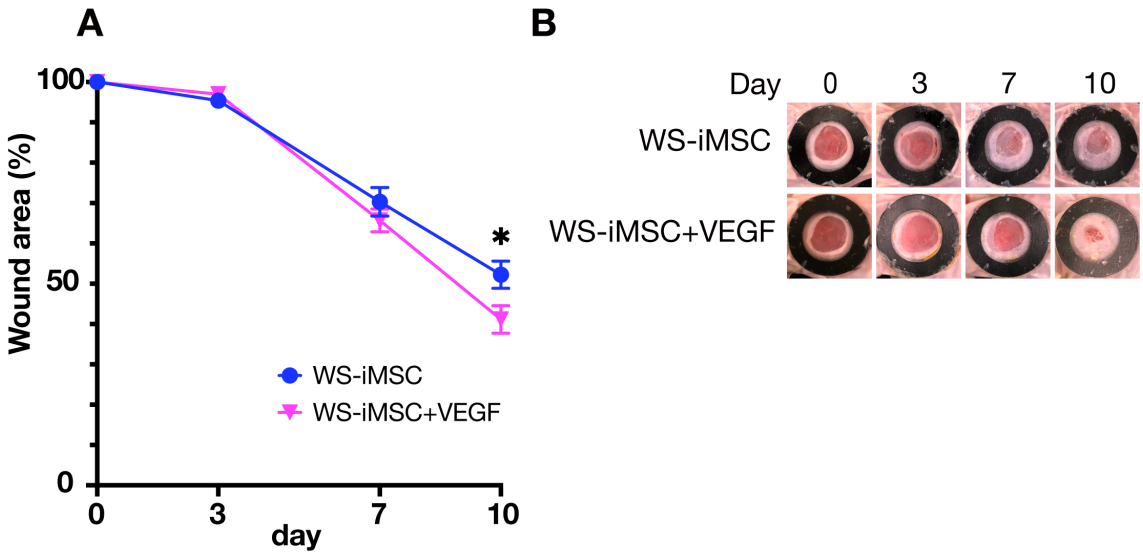

539
540 Figure 7. Wound healing effects of administration of WS-iMSC alone or WS-iMSC plus VEGF
541 on intractable skin ulcers.
542 (A) Graph showing the rate of wound area from day 0 to 10. Data are mean ± SEM (n = 7). A
543 student t-test was performed (*p<0.05). (B) Representative pictures of wounds on mice in each
544 group.
545

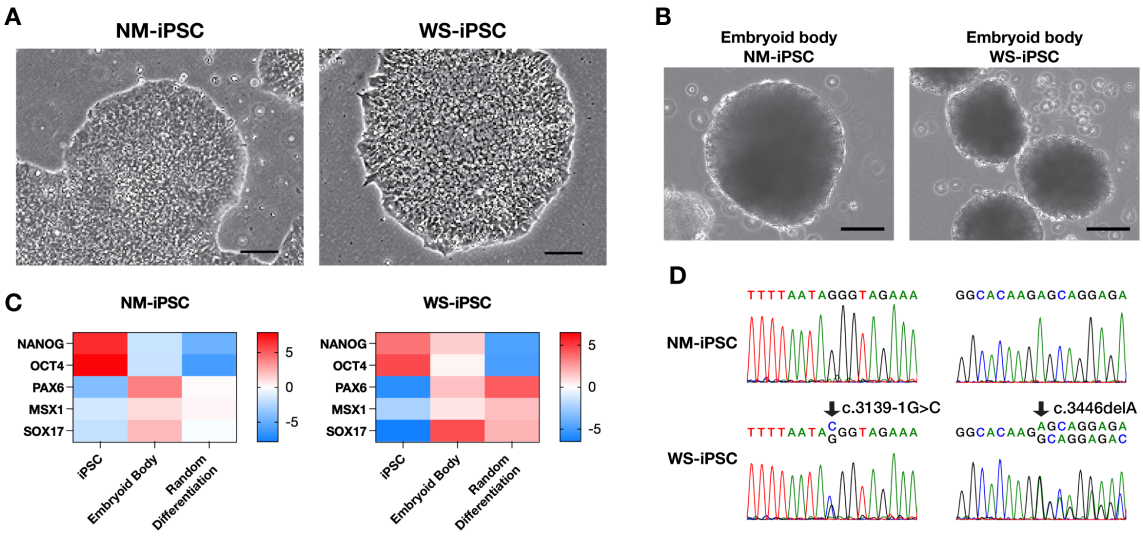

Supplementary Figure 1. Characteristics of NM- and WS-iPSC.

(A) Representative images of iPSCs. Bar = 100μm. (B) Representative images of embryoid bodies. Bar = 100μm. (C) Heatmap of qRT-PCR results assessing genes of pluripotency and three germ layers. (D) Sanger sequencing results at *WRN* mutated locus.

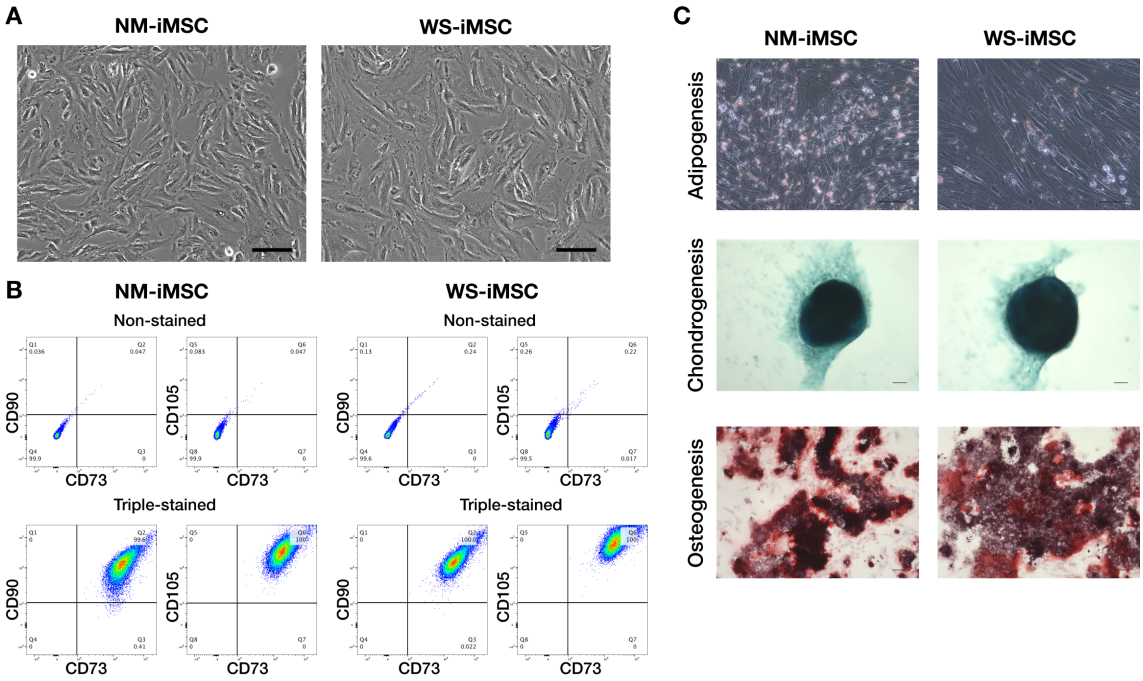

553

554 Supplementary Figure 2. Characteristics of NM- and WS-iMSC.

555 (A) Representative images of iMSCs at PD8. Bar = 100 μm. (B) FACS quantification of positive

556 cell rates for cell surface markers specific to MSCs. (C) Representative images of tri-lineage

557 differentiated cells. For staining, oil red O to adipogenesis, alcian blue to chondrogenesis, and

558 alizarin red to osteogenesis were used. Bar = 100 μm.

559

560

561 Supplementary Table. A list of the top 2000 genes with the highest SD in RNA-sequence of NM-

562 and WS-iMSC.

563